Scientific Eminence Group

Research Article

Journal of Traditional, Complementary & Alternative Medicine

Open Access

JTCA@scientificeminencegroup.com

Regulation and Analgesic Mechanism of Pivot Meridian Tuina on the Deubiquitinase OTUB1-mediated mTORC1 Signaling Pathway in Neuropathic Pain Rats

Tang Hongliang*

Affiliated Fangchenggang Hospital, Guangxi University of Chinese Medicine, Fangchenggang 538001, China

*Corresponding Author

Tang Hongliang, Affiliated Fangchenggang Hospital, Guangxi University of Chinese Medicine, Fangchenggang 538001, China, E-mail: tanghl2004@gxtcmu.edu.cn

Citation

Tang Hongliang (2024) Regulation and Analgesic Mechanism of Pivot Meridian Tuina on the Deubiquitinase OTUB1-mediated mTORC1 Signaling Pathway in Neuropathic Pain Rats. J Traditional Complement Altern Med 2: 1-22

Publication Dates

Received date: April 21, 2024

Accepted date: May 21, 2024

Published date: May 24, 2024

Abstract

Objective: To examine the influence of Pivot Meridian Tuina on the deubiquitination status of mTORC1 (Mammalian target of rapamycin complex 1) mediated by the deubiquitination enzyme OTUB1 (OUT Deubiquitinase,Ubiquitin Aldehyde Binding 1) in rats with neuropathic pain (NPP) and elucidate its analgesic molecular mechanism.

Methods: Fifty-six SPF (Specific pathogen Free) grade SD (sprague-dawley) rats were randomly divided into seven groups (n=8 each): model, blank control, Pivot Meridian Tuina, sham massage, sham operation, OTUB1 overexpression, and negative control (NC) groups. Except for the blank control and sham operation groups, the remaining five groups underwent L_5 spinal nerve ligation (SNL) for modeling. Post-modeling, the OTUB1 overexpression and NC groups were intrathecally injected with OTUB1 overexpression adenovirus and NC reagent, respectively. Mechanical stimulation contraction threshold (PWMT) and thermal pain contraction latency (PWTL) were measured in all groups before surgery (day 0) and on days 1, 3, and 14 post-operation. Pivot Meridian Tuina and sham massage interventions commenced on the first day post-operation and continued for 14 days. The remaining five groups were observed without intervention for 14 days. On the 14th day post-operation, the expression levels of OTUB1, DEPTOR, mTORC1 protein, ULK1 complex, serum interleukin (IL)-1β, and the ubiquitination status of DEPTOR protein was assessed.

Results: (1) Fourteen days post-operation, a decrease in the mechanical pain threshold was observed in the model, sham massage, and NC groups (P<0.05) compared to the blank control, Pivot Meridian Tuina, sham operation, and OTUB1 overexpression groups. The thermal pain threshold increased in the blank control, Pivot Meridian Tuina, and OTUB1 overexpression groups compared to the model, sham massage, and NC groups (P<0.05). (2) The expression of OTUB1 increased in the Pivot Meridian Tuina, sham massage, and OTUB1 overexpression groups compared to the blank control and model groups. Additionally, mTORC1 expression was elevated in the model and NC groups relative to the blank control and Pivot Meridian Tuina groups (P<0.05). However, the expression of DEPTOR increased among the groups (P>0.05). (3) Ubiquitination levels increased in the Pivot Meridian Tuina and OTUB1 overexpression groups compared to the blank control, NC, and model groups (P<0.05). (4) The expression of ULK1 increased in the Pivot Meridian Tuina and OTUB1 overexpression groups compared to the sham operation, NC, and sham massage groups. The levels of FIP200 increased in the Pivot Meridian Tuina and OTUB1 overexpression groups compared to the blank control, sham operation, NC, and model groups (P<0.05). (5) Both the Pivot Meridian Tuina and the OTUB1 overexpression groups exhibited notably decreased serum IL-1β expression levels compared to the NC, model, and sham massage groups (P<0.05).

Conclusion: Pivot Meridian Tuina intervention alleviates hyperalgesia symptoms in SNL rats, possibly attributed to the upregulation of the deubiquitination enzyme OTUB1, which leads to the inhibition of DEPTOR ubiquitination. Consequently, this enhances DEPTOR stability, thereby inhibiting the activity of downstream mTORC1 protein. This subsequently leads to increased expression of the ULK1 complex, promoting autophagy and reducing the expression of the inflammatory factor IL-1β.

Keywords: Pain; Neuropathic pain; Massage; Pivot Meridian Tuina; Deubiquitination; Deubiquitinating enzyme OTUB1; mTOR pathway; Analgesia; Rat

Introduction

Neuropathic pain (NPP) results from nervous system impairment or disease [1]. In recent years, experts and scholars worldwide have increasingly recognized pain as the fifth vital sign. Clinically, NPP has a high incidence. The World Health Organization estimates an incidence of 6.9–10% [2,3]. Current clinical treatments for NPP are predominantly palliative, relying on major drugs such as opioids [4], gabapentinoids [5], and nonsteroidal anti-inflammatory drugs [6]. However, the effectiveness of these treatments is unsatisfactory, primarily due to the unclear understanding of NPP's pathogenesis.

The Pivot meridian tuina is grounded in the theoretical framework of the "the Pivot Meridian Theory," with its core essence revolving around the "pivoting" concept. The "Pivot Meridian" encompasses four meridians: the heart meridian of hand-shaoyin, the kidney meridian of foot-shaoyin, the triple energizer meridian of hand-shaoyang, and the gallbladder meridian of foot-shaoyang. Each meridian plays a role in guiding other meridians and internal organs within the body. Pivot meridian tuina therapy aims to facilitate the smooth flow of the "Pivot Meridian," thereby promoting balanced qi circulation throughout the body, both internally and externally, and fostering equilibrium between the yin and yang. Ultimately, this therapeutic approach strives to maintain normal physiological functions in the body. Our previous studies have demonstrated that Pivot meridian tuina effectively reduces the release of inflammatory factors, including interleukin (IL)-1β and IL-6, contributing to its analgesic effects [7,8]. However, the precise mechanism underlying this effect remains unclear. An increasing number of studies have demonstrated that

OTUB1 (OUT Deubiquitinase, Ubiquitin Aldehyde Binding 1) can suppress the secretion of inflammatory factors, including IL-1β and IL-10, thereby mitigating the inflammatory response [9].

Herein, Pivot meridian tuina was employed to treat rats with NPP. We initially focused on the deubiquitylase OTUB1, aiming to elucidate the molecular mechanisms underlying the analgesic effects of Pivot meridian tuina, provide insights into epigenetic deubiquitination, and offer a novel method and target for NPP treatment.

1. Experimental Materials

1.1 Experimental Animals

Fifty-six healthy adult female SD (sprague-dawley) rats (6–8 weeks, weighing 220–250 g) were obtained from Hunan SJA Laboratory Animal Co., Ltd. (production license no. SCXK [Xiang] 2019-0004, use license no. SYXK [Gui] 2019-0001). Each rat was individually housed in a cage for 7 days under controlled room temperature (20–25℃) and humidity (35–45%). The rats had unrestricted access to tap water and were fed plain, clean chow. Cages and bedding were changed daily. All experimental procedures strictly adhered to the regulations established by Guangxi University of Chinese Medicine regarding the feeding, handling, and utilization of experimental animals. The experiments involving pain assessment in conscious animals strictly followed established guidelines. (approval no. DW20230302-017).

1.2 Experimental Consumables

RNase-free gun head was procured from Axygen (Silicon Valley, California, USA). Centrifuge tubes (15 and 50 mL) and EP (Eppendorf) tubes were obtained from Thermo (Waltham, Massachusetts , USA). PVDF (PolyVinylidene-Fluoride) membrane was procured from Merck Millipore (American Massachusetts). Other consumables, such as standard filter paper, were domestically acquired.

2. Experimental Reagents

2.1 Antibodies

We employed antibodies against the following: OTUB1 (3783S, CST), DEPTOR (DEP domain-containing mTOR-interacting protein) (11816S, CST), mouse IgG (5415S, CST), mTORC1 (Mammalian target of rapamycin complex 1) (10441-1-AP, Proteintech), ubiquitin (UB) (10201-2-AP, Proteintech), ATG13 (autophagy related protein 13) (18258-1-AP, Proteintech Group, Inc), RB1CC1/FIP200 (FAK-family interacting protein of 200 kDa) (17250-1-AP, Proteintech), ULK1 (unc-51-like kinase 1) (A00584-1, BOSTER), β-actin (TA-09, ZSGB-BIO), Horseradish Peroxidase -conjugated Affinipure goat anti-mouse IgG (H+L) (ZB-2305, ZSGB-BIO), and HRP-conjugated Affinipure goat anti-rabbit IgG (H+L) (ZB-2301, ZSGB-BIO).

2.2 Primary Reagents

We employed the following materials: an immunoprecipitation kit (Sangong Biotech (Shanghai) Co., Ltd., C600689), methanol (67-56-1, Xilong Science Co., Ltd.), Tween-20 (T8220, Solarbio), bovine serum albumin (A8020, Solarbio), Tris (T8060-500 g, Solarbio), glycine (G8200-500 g, Solarbio), 30% acrylamide (A1010-500 mL, Solarbio), SDS (Sodiumdodecyl sulfate) (S8010-500 mL, Solarbio), 20× TBST buffer (T1082-500 mL, Solarbio), TEMED （N,N,N',N'-Tetramethylethylenediamine） (T8090, Solarbio), rapid isolation of proteins from aqueous humor (RIPA) lysis buffer (high) (R0010, Solarbio), NaCl (7647-14-5, Damao Chemical Reagent Factory, Tianjin), KCl (Tianjin Zhiyuan Chemical Reagent Co., Ltd.), skimmed milk powder (P1622, Beijing Applygen Technologies Inc.), QuickBlock™ Western Containment Solution (P0252-500 ml, Beyotime Biotech Inc.), a BCA protein concentration measurement kit (P0010S, Beyotime Biotech Inc.), an SDS- PAGE（Sodium dodecyl sulphate-polyacrylamide gel electrophoresis） loading buffer (P0015, Beyotime Biotech Inc.), a multicolor prestained protein ladder (WJ003, Shanghai Yamay Biomedical Technology Co., Ltd.), an enzyme linked immunosorbent assay (ELISA) kit for rat IL-1β (F2923-A, Shfksc). These materials encompassed buffers, chemicals, kits, and reagents employed in various laboratory procedures, including immunoprecipitation, protein analysis, and ELISA.

2.3 Customized Adenovirus Overexpression

The cloning templates for OTUB1 overexpression adenovirus were acquired from a clone library at Shanghai Genechem Co., Ltd.

2.4 Primary Instruments

The instruments employed in our experiments included: a single channel adjustable volume pipette (Eppendorf), the YI-875 Clean Bench (Suzhou Purification Equipment Factory), a multimode microplate reader (Infinite M200 PRO, Beijing Long Jump Biological Science and Technology Development Co., Ltd.), a low-temperature high-speed centrifuge (5424R, Eppendorf), an electric-heated thermostatic water bath (HH-11-2, Shanghai Zhulan Instrument Technology Co., Ltd.), a protein vertical electrophoresis Instrument (DYY-6C, Beijing Liuyi Instrument Factory), a thermostatic shaker (TC-100B, Shanghai Tocan Biotechnology Co., Ltd.), a chemiluminescent image analysis system (Tanon-5200, Tanon Science & Technology Co., Ltd., Shanghai), Von Frey filaments (BW806, Shanghai Biowill Co., Ltd.), and a hot plate analgesia test meter for mice and rats (IITC Corporation, USA).

3. Research Methodology

3.1 Grouping of Experimental Animals

Rats were randomly stratified into seven groups employing the random number table method: model, blank control, Pivot Meridian Tuina, sham massage, sham operation, OTUB1 overexpression, and negative control (NC) groups (n=8 each).

3.2 Establishment of a Spinal Nerve Ligation (SNL) Model

During the initial research phase [10], we performed surgical procedures on the model, Pivot Meridian Tuina, sham massage, OTUB1 overexpression and NC groups to establish an SNL rat model . Before the surgery, all rats in each group underwent a 12-h fasting period, and their weights were recorded. Anesthesia was intraperitoneally injected (a dosage of 0.35 mL of 1% pentobarbital sodium per 100 g of body weight). The disappearance of the corneal reflex indicated successful anesthesia. Subsequently, the rats were positioned in a prone posture, with their heads and limbs immobilized. The posterior superior iliac spine on both sides was aligned, and the surgical site was prepared by shaving the skin and implementing standard disinfection protocols. A longitudinal incision (approximately 2 cm in length) was created between the left posterior superior iliac spine and the spine, running parallel to the spinal direction. Tissue layers were gently separated through blunt dissection, exposing the L_4 and L_5 spinal nerves by separating the transverse processes using a rongeur. Next, the L_5 nerve was gently separated and ligated using double layers of 5-0 absorbable catgut sutures. The wound was subsequently cleaned and sutured.

Rats in the OTUB1 overexpression group and NC group were subjected to intrathecal injection after modeling. The blank control group received no treatment. Rats in the sham operation group underwent a procedure identical to the aforementioned method, except that the L_5 spinal nerves were briefly exposed for a few minutes without ligation.

3.3 Intrathecal Injection

The method for intrathecal injection involved the following steps [11]: After the preparation of the SNL model, the OTUB1 overexpression group and the negative control group rats were compared, we positioned a 20-mL syringe beneath their abdomen to fully expose the lumbar intervertebral space. Following limb fixation, an aseptic hole-towel was used to cover the surgically prepared area. A midpoint was marked on the line connecting the two sides of the anterior superior iliac spines, and a 2–3 cm longitudinal incision was created at the middle of the L_5-L_6 spinal level, allowing for the separation of paravertebral muscles and fascia down to the vertebral plate. Subsequently, a 20G needle with a flattened tip was carefully inserted into the punctured intervertebral space, directed towards the rat's head. When the needle penetrated the subarachnoid space, the rat exhibited temporary tail or hind limb twitching. At this point, a PE10 catheter was slowly inserted in the same direction and angle as the needle, using tweezers, to a depth of approximately 3 cm. The needle was then withdrawn. Once clear and transparent cerebrospinal fluid was observed flowing from the catheter, after use a 10 μL microinjection needle to aspirate 10 μL of adenovirus and negative control reagent, and inject them through a PE10 catheter. At this time, the rat will once again experience transient tail flick, indicating successful injection. After flushing the catheter with sterile physiological saline (10 uL), we sutured each surgical incision sequentially. Afterward, the rats were individually housed in separate cages, and the same individual who conducted the operation oversaw this phase.

3.4 Intervention Methodology

3.4.1 Pivot Meridian Tuina group

After the rats had calmed, the bilateral Shaoyang gallbladder meridian was stimulated, targeting the Huantiao, Yanglingquan, and Xuanzhong points. The simulation techniques included pointing, dialing, and kneading (4 N force). Each massage method was applied to each location for 1 min, resulting in a total duration of 18 min (bilaterally) per rat. This intervention was administered daily for 14 days.

3.4.2 Sham Massage Group

After the rats had calmed, the operator's right hand gently caressed both hind limbs of the rats for 18 min. This intervention continued for 14 days.

3.5 Assessment of Pain Behavior in Rats

3.5.1 Measurement of Paw Withdrawal Mechanical Threshold (PWMT) in Rats

The PWMT of rats in each group was assessed at multiple time points: 0 days pre-operatively and 1 day, 3 days, and 14 days postoperatively [12]. Rats were housed in cages with four layers of wire mesh flooring, maintained at 25℃. After a 30-min acclimatization period, the von Frey fiber was employed to stimulate the mid-plantar area of the operated hind limb. This stimulation involved gradually increasing the applied force in sequential steps. Each stimulation event lasted for 5 s, with termination upon the observation of a positive response. Furthermore, the test was conducted five times for each von Frey fiber type. If rats exhibited paw withdrawal or paw licking three or more times, it was deemed a positive response; otherwise, it was considered a negative response. The minimum hindpaw withdrawal threshold of the rats was recorded. Following the initial measurement, a second measurement was taken after a 5-min interval to avoid injury. This procedure was repeated three times, and the final result was calculated as the average value across these three tests.

3.5.2 Measurement of Paw Withdrawal Thermal Latency (PWTL) in Rats

The PWTL of rats in each group was assessed at four time points: 0 days prior to the operation and 1, 3, and 14 days post-operation [13]. The room temperature was 25 ℃, and the hot plate analgesia tester was calibrated to precisely 55±0.2℃. Rats were placed inside a closed, transparent glass box within the tester, and the timer was initiated. The timer was stopped when the rats exhibited rapid paw lifting and frequent paw licking, and this behavior was recorded. Three consecutive measurements were taken, each separated by a 5-min interval. The PWTL was determined by calculating the average value of these measurements, indicating the response time of the rats to thermal stimuli. A quiet atmosphere and a calm operating environment were maintained to avoid alarming the rats. Moreover, a safety precaution was implemented to protect the rats from potential burns, which involved setting a cut-off time of 30 s.

3.6 Sample Collection

After 2 h of behavioral observation on the 14th postoperative day, rats from each group were anesthetized and blood was drawn from the abdominal aorta. Subsequently, spinal cord tissues from the L4–L6 region were quickly harvested, rapidly cooled in liquid nitrogen, and stored at -80℃ for preservation.

3.7 Molecular Assessments

3.7.1 Western Blot Analysis of OTUB1, DEPTOR, and Mtorc1 Proteins in the Spinal Cord

The appropriate amount of spinal cord tissue was collected, as described in Section 3.6. For grinding and homogenization, an adequate volume of RIPA lysis buffer (high) was utilized. The resulting mixture was centrifuged (12,000×g 15 min, 4℃). Next, the supernatant was carefully separated, and the protein concentration was determined using a BCA kit. The protein loading buffer was then added to the samples, and the prepared samples were stored at -20℃. The amount of protein loading buffer was adjusted based on the protein concentration, followed by electrophoresis. Electrophoresis was conducted at 80 V for 40 min, with an increase to 120 V until bromophenol blue reached the bottom of the gel. Subsequently, a 200-mA electrophoretic transfer was performed for 1 h. Moreover, the PVDF membrane was sealed with a sealing solution at room temperature for 15 min and then incubated overnight at 4℃ with the following primary antibodies: an-

ti-OTUB1 (1:1,000), anti-DEPTOR (1:1,000), anti-mTORC1 (1:1,000), and anti-β-actin (1:2,000), respectively. The membrane underwent three 10-min washes with 1× TBST buffer. Subsequently, it was incubated with an HRP-labeled secondary antibody (1:10,000 dilution) at 25℃ for 1 h. Next, the membrane was washed thrice with 1× TBST buffer for 10 min each time. Luminescence was developed using an ECL (enhanced chemiluminescence) reagent, and the grayscale intensity of the bands was analyzed using ImageJ software. This experiment was repeated three times for validation.

3.7.2 Detection of the Ubiquitination Status of DEPTOR and the Protein Levels of the ULK1 Complex in Spinal Cord Tissues *via* co-immunoprecipitation (Co-IP)

Protein A/G Plus-Agarose (20 μL) was added to a filter-containing column, and 1× PBS（Phosphate buffer saline）(700 μL) was used for agarose washing. The mixture was centrifuged at low speed, and this washing process was repeated four times to ensure adequate preparation of the agarose. Tissue (approximately 60 mg) was taken and washed twice with pre-cooled PBS. Subsequently, 1× lysis buffer (1 mL), diluted with double-distilled water, was added. The mixture was placed on ice and homogenized using a homogenizer. After gentle mixing and lysis at 4℃ for 30 min, it was centrifuged (12,000 rpm, 10 min) to collect the supernatant. A portion of this supernatant was retained as input for detecting the expression of DEPTOR, UB, β-actin, ATG13, ULK1, and RB1CC1/FIP200. In a new microcentrifuge tube, the lysate (0.7 mL), along with anti-PMSF (Phenylmethanesulfonyl fluoride) (7 μL), anti-DEPTOR (1 μg), and anti-ATG13 antibodies (with IgG protein serving as the NC antibody), were added. Next, the mixture was incubated on a platform (4℃, 4 h). Then, the lysate was transferred to a previously washed Protein A/G Plus-Agarose-containing column and incubated overnight on the platform (4℃). Subsequently, the contents of each column were transferred into separate 2-mL microcentrifuge tubes. They were then centrifuged (12,000 rpm, 30 s, 4℃). The supernatant was removed, and the agarose beads were precipitated and washed six times with 1× IP (Immunoprecipitation) buffer (700 μL), followed by one to two washes with 0.1× IP buffer (700 μL). Finally, the beads were centrifuged (12,000 rpm, 30 s). To the washed beads, 1× loading buffer (50 μL) was added and gently mixed. The mixture was then heated (95°C, 5 min). After removing excess water around the lid using filter paper, we inserted the column into a new microcentrifuge tube and centrifuged it (12,000 rpm, 30 s). The eluted co-IP samples were subjected to SDS-PAGE for subsequent western blot analysis.

3.8 Detection of Serum IL-1β *via* ELISA

Blood was obtained from the abdominal aorta of rats in each group and centrifuged (3,000 rpm, 15 min, 4℃). The upper layer containing serum was collected. Serum IL-1β levels were assessed using an ELISA kit, and this procedure was repeated three times. Moreover, the absorbance value was measured at a wavelength of 450 nm using an enzyme-labeled instrument.

3.9 Statistical Analysis

All experimental data were statistically analyzed using SPSS 22.0. Measurement data were expressed as mean ± standard deviation (x±s). For comparisons among multiple groups influenced by two factors, we employed repeated-measures analysis of variance (ANOVA). In the case of a single group of influencing factors, we conducted mean comparisons of the means of multiple groups using one-way ANOVA, along with the homogeneity of variance test. If homogeneity of variance was confirmed, the LSD（least significant difference） test was utilized for pairwise group comparisons. Meanwhile, for cases with heteroscedasticity, we employed Dunnett's C method for pairwise comparisons between groups. When measurement data deviated from a normal distribution, it was presented as median ± quartile (M_0±d). P<0.05 indicated a statistically significant difference.

4. Experimental Results

4.1 Changes in PWMT in Each Group

Before the surgery, no statistically significant difference was observed in the PWMT among the rats in all groups (P>0.05). However, on the first and third days after the surgery, the PWMT in each experimental group, except the blank control group, was lower (^{a}P<0.05). On the third day post-surgery, the PWMT in the model, Pivot Meridian Tuina, sham massage, and NC groups was markedly lower than that in the sham operation group (^{bcde}P<0.05). Relative to that in the model and NC groups, the PWMT was notably higher in the

OTUB1 overexpression group ($^{ce}P<0.05$). However, by the 14th day after surgery, the PWMT in the model, sham massage, and NC groups had decreased compared to the blank control, Pivot Meridian Tuina, sham operation, and OTUB1 overexpression groups ($P<0.05$).

Table 1: changes of mechanical pain threshold in rats of each group ($\bar{x}\pm s$, g, n=8)

Section	Before operation	1 day after operation	3 day after operation	14 day after operation
Model group	41.17±8.58	0.24±0.05^{a}	0.59±0.21^{a}	2.50±0.85^{ab}
Blank control group	41.17±8.58	46.00±9.09	35.50±7.94	41.17±8.58
Massage group	46.83±8.45	0.42±0.13^{a}	5.00±1.44^{a}	34.67±8.40
Sham massage group	41.17±8.58	0.66±0.27^{a}	2.57±0.46^{a}	14.00±2.67^{ab}
Sham operation group	48.67±7.17	8.83±1.38^{a}	20.33±3.59^{abcde}	41.17±8.58^{cde}
Otub1 overexpression group	46.00±9.09	5.90±3.93^{a}	13.00±4.22^{ace}	38.50±9.84^{cde}
Negative control group	46.83±8.45	0.35±0.17^{a}	0.73±0.12^{a}	1.13±0.59^{ab}

Note: $F_{group}=13.409$, $P_{group}=0.000$; $F_{time}=51.943$, $P_{time}=0.000$; $F_{group*time}=2.976$, $P_{group*time}=0.002$, compared with the blank control group $^{a}P<0.05$, compared with massage group $^{b}P<0.05$, compared with model group $^{c}P<0.05$, compared with sham massage group $^{d}P<0.05$, compared with negative control group $^{e}P<0.05$.

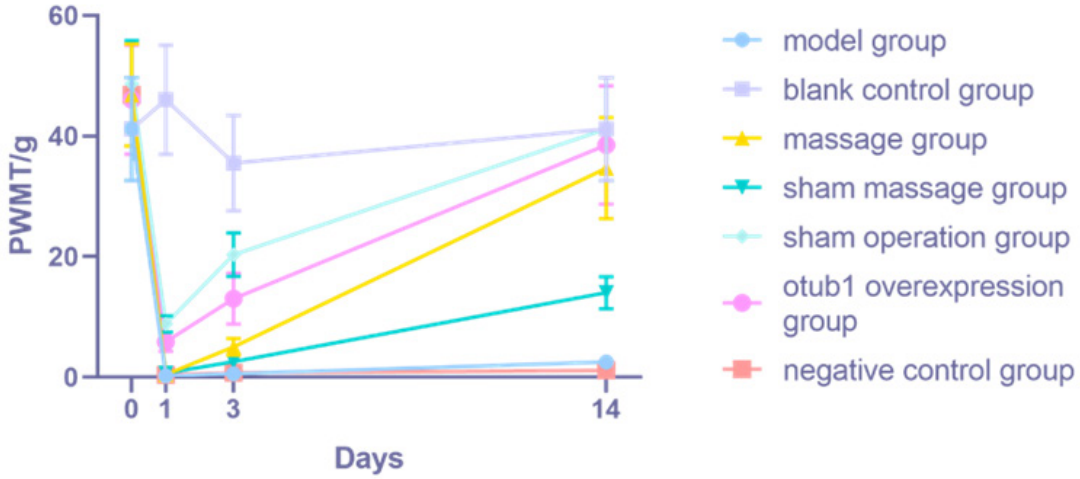

Figure 1: changes of mechanical pain threshold in rats of each group

4.2 Changes in PWMT in Each Group

Before the surgery, no statistically significant differences were observed in the PWMT among the groups. ($P>0.05$). However, on the first and third postoperative days, the PWMT in the other groups was lower compared to that in the blank control group ($^{a}P<0.05$). The PWMT in the Pivot Meridian Tuina, model, sham massage, and NC groups was lower compared to the sham operation and OTUB1 overexpression groups ($^{bcde}P<0.05$). By the third postoperative day, an increase in PWMT was observed in the Pivot Meridian Tuina group ($^{b}P<0.05$) compared to the model and sham massage groups. After 14 postoperative days, the PWMT in the model, sham massage, sham operation, and NC groups remained low-

er compared to the blank control and Pivot Meridian Tuina groups ($^{ab}P<0.05$). The PWMT in the sham massage and NC groups was elevated compared to the model group ($^{c}P<0.05$). The sham operation and OTUB1 overexpression groups exhibited an elevated PWMT compared to the model, sham massage, and NC groups ($^{cde}P<0.05$).

Table 2: changes of thermal pain threshold in rats of each group ($\bar{x}$ ±s, s, n=8)

Section	Before operation	1 day after operation	3 day after operation	14 day after operation
Model group	26.32±1.01	4.50±0.38^{a}	5.54±0.40^{ab}	11.19±1.15^{ab}
Blank control group	27.13±0.77	27.38±0.84	27.16±0.73	28.04±0.56
Massage group	27.10±0.89	5.09±0.36^{a}	8.33±0.54^{a}	27.49±0.54
Sham massage group	26.42±1.77	5.09±0.39^{a}	6.50±0.28^{ab}	14.23±0.74^{abc}
Sham operation group	26.90±1.03	9.20±0.50^{abcde}	12.27±0.92^{abcde}	18.42±0.55^{abcde}
Otub1 overexpression group	27.10±0.83	9.72±0.60^{abcde}	14.13±0.72^{abcde}	26.70±0.92^{cde}
Negative control group	26.48±0.80	6.66±0.52^{abcd}	7.94±0.47^{ac}	13.88±0.30^{abc}

Note: $F_{group}=258.041$, $P_{group}=0.000$；$F_{time}=686.136$, $P_{time}=0.000$；$F_{group*time}=32.984$, $P_{group*time}=0.000$, compared with the blank control group $^{a}P<0.05$, compared with massage group $^{b}P<0.05$, compared with model group $^{c}P<0.05$, compared with sham massage group $^{d}P<0.05$, compared with negative control group $^{e}P<0.05$.

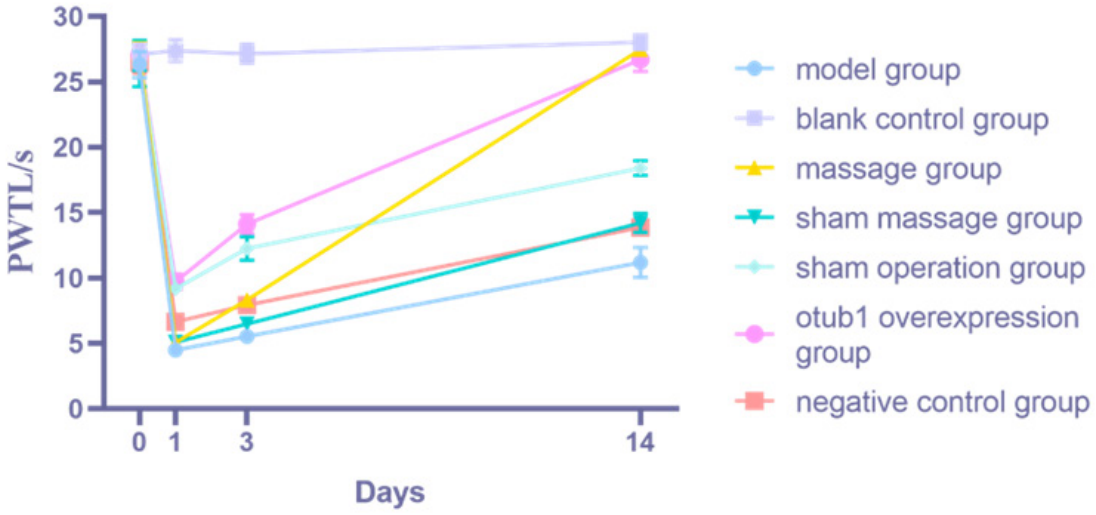

Figure 2: changes of thermal pain threshold in rats of each group

4.3 Comparitive Analysis of OTUB1, DEPTOR, and Mtorc1 Protein Expression in Rat Spinal Cord Tissues

On the 14th postoperative day, OTUB1 expression was elevated in the Pivot Meridian Tuina, sham massage, and OTUB1 overexpression groups compared to the blank control and model groups. Additionally, OTUB1 expression was elevated in the OTUB1 overexpression group compared to the sham massage and NC groups. Moreover, mTORC1 expression was elevated in the model and NC groups compared to the blank control and Pivot Meridian Tuina groups. Similarly, mTORC1 expression in the sham massage and OTUB1 overexpression groups was lower than that in the model group, with the

OTUB1 overexpression group exhibiting lower mTORC1 expression compared to the NC group. These observed differences were statistically significant (P<0.05). However, DEPTOR expression did not exhibit statistically significant differences (*P*>0.05) among all the groups.

Table 3: Comparison of protein expression levels of OTUB1, DEPTOR and mTORC1 in spinal cord tissues of rats in each group ($\bar{x}$±s, n=8)

Section	OTUB1/β-actin	DEPTOR/β-actin	mTORC1/β-actin
Model group	0.42±0.12[b]	0.63±0.15	1.11±0.11[ab]
Blank control group	0.47±0.70	0.66±0.17	0.50±0.08
Massage group	0.91±0.01[a]	0.91±0.13	0.62±0.05
Sham massage group	0.74±0.03[ac]	0.81±0.38	0.76±0.11[c]
Sham operation group	0.65±0.01[b]	0.63±0.29	0.87±0.16[a]
Otub1 overexpression group	1.30±0.06[abcde]	0.91±0.09	0.51±0.04[ce]
Negative control group	0.61±0.14[b]	0.53±0.05	0.98±0.11[ab]
F value	14.473	1.410	5.439
P value	0.000	0.278	0.004

Note: compared with the blank control group [a]P<0.05, compared with massage group [b]P<0.05, compared with model group [c]P<0.05, compared with sham massage group [d]P<0.05, compared with negative control group [e]P<0.05.

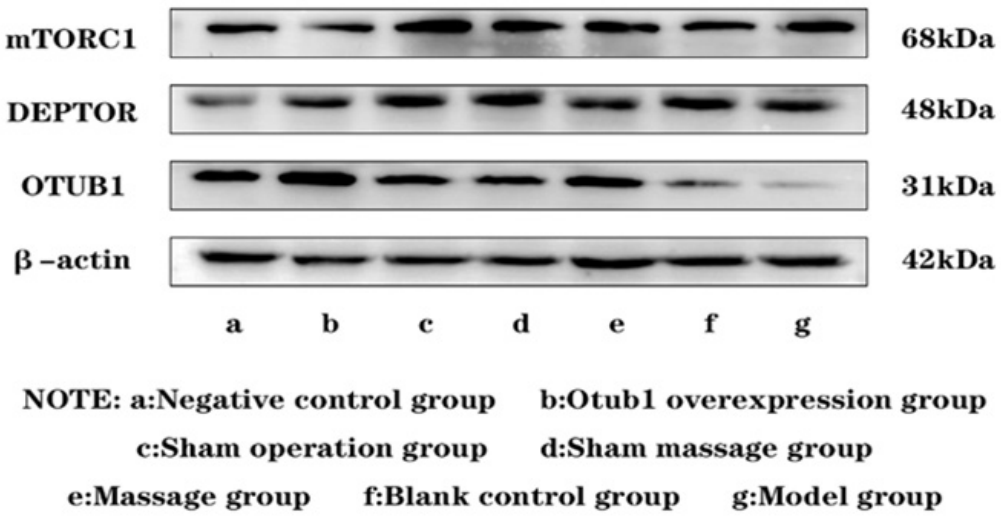

Figure 3: Comparison of protein expression levels of OTUB1, DEPTOR and mTORC1 in spinal cord tissues of rats in each group

4.4 Comparative Analysis of the Ubiquitination Status of DEPTOR in Rat Spinal Cord Tissues

On the 14th postoperative day, both the Pivot Meridian Tuina and OTUB1 overexpression groups exhibited higher levels of ubiquitination compared to the blank control, NC, and model groups ([abc]*P*<0.05). Likewise, the Pivot Meridian Tuina group demonstrated increased ubiquitination levels compared to the sham massage group ([d]*P*<0.05).

Table 4: Comparison of ubiquitination levels in spinal cord tissue of rats in each group ($\bar{x}\pm s$, n=8)

Section	Ubiquitination level
Blank control group	0.69±0.07
Sham operation group	0.80±0.14
Negative control group	0.52±0.11
Model group	0.67±0.12
Sham massage group	0.76±0.14
Massage group	1.22 ± 0.16^{abcd}
Otub1 overexpression group	1.17 ± 0.22^{abc}
F value	3.270
P value	0.032

Note: compared with the blank control group $^{a}P<0.05$, compared with negative control group $^{b}P<0.05$, compared with model group $^{c}P<0.05$, compared with sham massage group $^{d}P<0.05$.

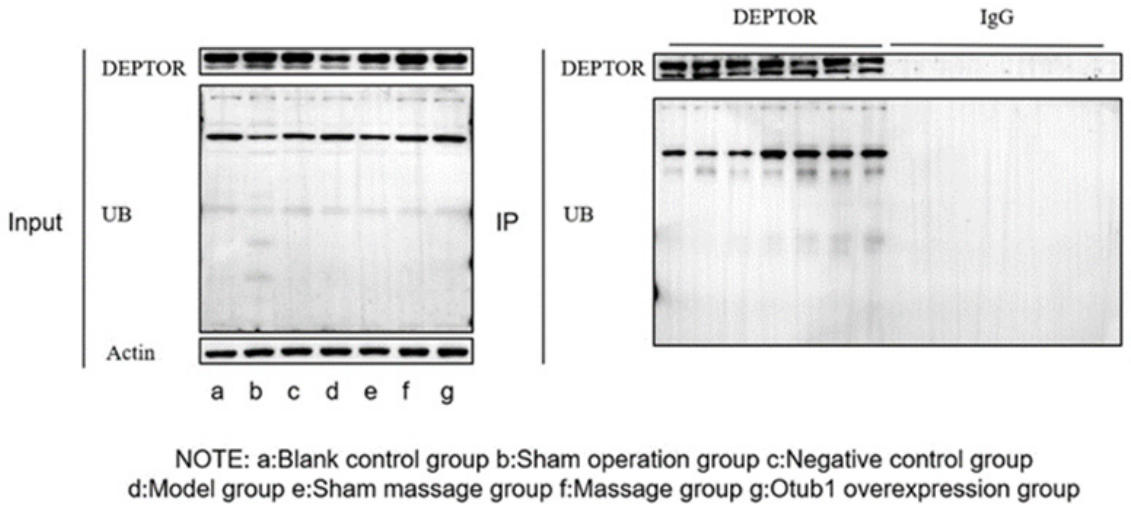

Figure 4: Comparison of ubiquitination levels in spinal cord tissue of rats in each group

4.5 Comparative Analysis of the Expression Levels of ULK1 Complex Proteins in Rat Spinal Cord Tissues

On the 14th postoperative day, ULK1 levels were significantly lower in the NC group compared to the blank control group ($^{a}P<0.05$). Moreover, ULK1 levels were elevated in the Pivot Meridian Tuina and OTUB1 overexpression groups relative to the sham operation, NC, and sham massage groups ($^{bcd}P<0.05$). Furthermore, ULK1 levels were elevated in the sham massage group compared to the NC group ($^{c}P<0.05$). Additionally, on the 14th postoperative day, FIP200 levels in the Pivot Meridian Tuina and OTUB1 overexpression groups were elevated ($^{abcd}P<0.05$) compared to the blank control, sham operation, NC, and model groups. Moreover, FIP200 levels in the sham operation and NC groups were lower ($^{a}P<0.05$) than those in the blank control group. Moreover, FIP200 levels were elevated in the sham massage group compared to the sham operation, NC, and model groups ($^{bcd}P<0.05$). Higher FIP200 levels were observed in the model group relative to the NC group ($^{c}P<0.05$). Lastly, the OTUB1 overexpression group exhibited elevated FIP200 levels compared to the sham massage group ($^{e}P<0.05$).

Table 5: Comparison of expression levels of ULK1 complex protein in spinal cord tissue of rats in each group ($\bar{x}$±s, n=8)

Section	ULK1/ATG13	FIP200/ATG13
Blank control group	0.46±0.09	0.59±0.11
Sham operation group	0.30±0.11	0.42±0.04[a]
Negative control group	0.17±0.08[a]	0.25±0.03[a]
Model group	0.27±0.09	0.43±0.06[c]
Sham massage group	0.51±0.08[c]	0.76±0.03[bcd]
Massage group	0.69±0.09[bcd]	0.90±0.03[abcd]
Otub1 overexpression group	0.70±0.07[bcd]	0.98±0.04[abcde]
F value	5.552	23.564
P value	0.004	0.000

Note: compared with the blank control group [a]P<0.05, compared with sham operation group [b]P<0.05, compared with negative control group [c]P<0.05, compared with model group [d]P<0.05, compared with sham massage group [e]P<0.05.

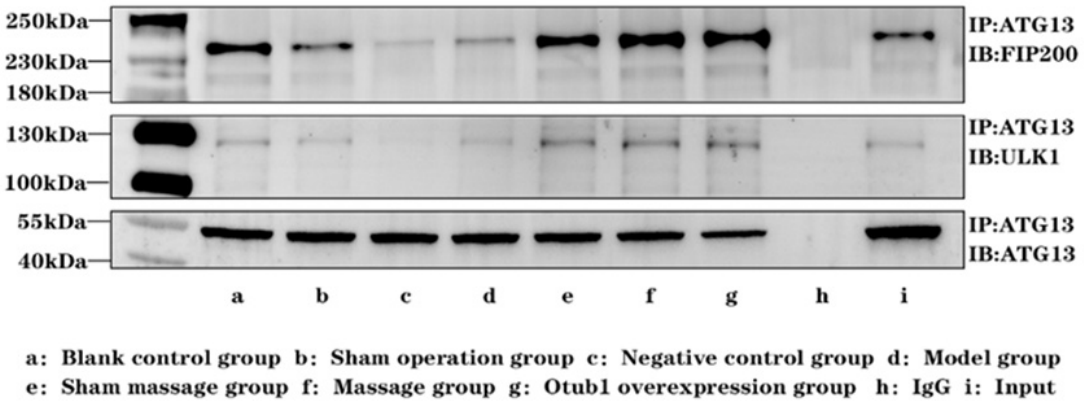

Figure 5: Comparison of expression levels of ULK1 complex protein in spinal cord tissue of rats in each group

4.6 Comparative Analysis of Rat Serum IL-1β Expression Levels on the 14th Postoperative Day

On the 14th postoperative day, serum IL-1β levels in all groups, except for the blank control group, were elevated (^{a}P<0.05). Similarly, compared to the sham operation group, the NC and the model groups exhibited elevated serum IL-1β levels (^{b}P<0.05). Serum IL-1β levels in the Pivot Meridian Tuina and OTUB1 overexpression groups were significantly lower than those in the NC, model, and sham massage groups (^{cde}P<0.05). In contrast to the model group, the sham massage group showed lower serum IL-1β levels (^{d}P<0.05).

Table 6: Comparison of serum IL-1β expression levels in rats of each group ($\bar{x}$±s, pg/ul, n=8)

Section	IL-1β level
Blank control group	319.28±20.20
Sham operation group	393.61±9.57[a]
Negative control group	451.92±5.23[ab]

Model group	480.70±6.25[ab]
Sham massage group	423.14±7.95[ad]
Massage group	366.58±5.00[acde]
Otub1 overexpression group	370.84±7.46[acde]
F value	30.014
P value	0.000

Note: compared with the blank control group [a]P<0.05, compared with sham operation group [b]P<0.05, compared with negative control group [c]P<0.05, compared with model group [d]P<0.05, compared with sham massage group [e]P<0.05.

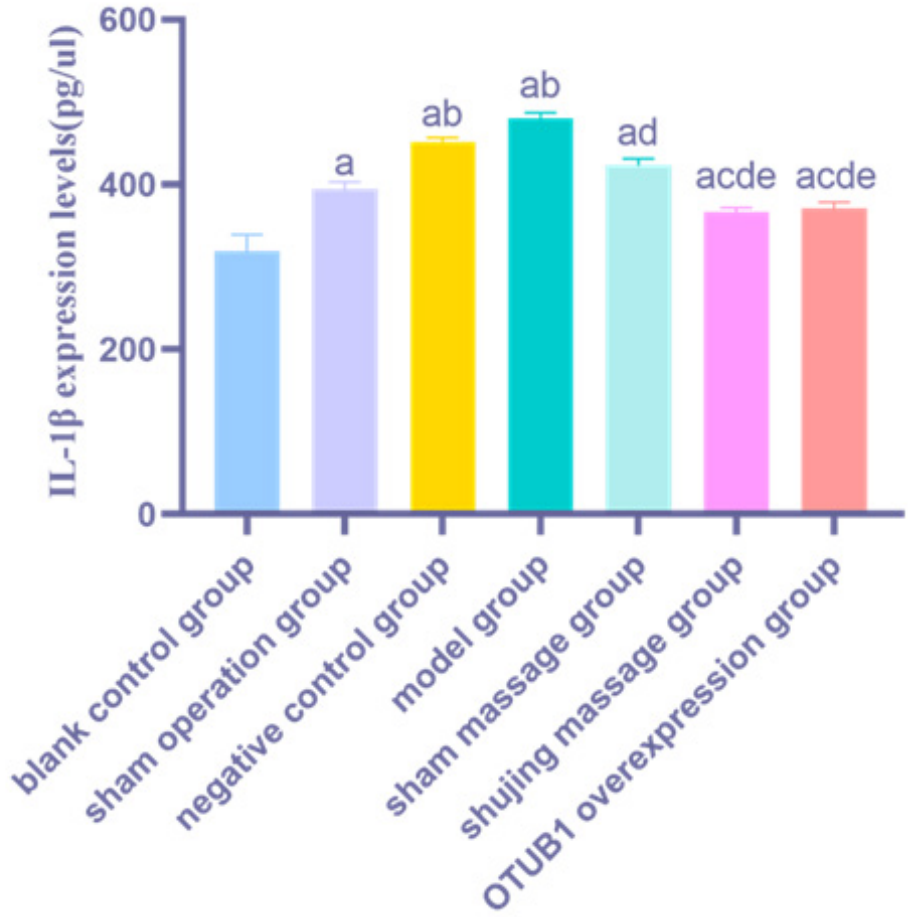

Figure 6: Comparison of serum IL-1β expression levels in rats of each group

5. Discussion

5.1 Theoretical Basis and Selection of acupoints for Pivot Meridian Tuina

NPP falls within the realm of modern medicine. In traditional Chinese medicine, it is classified as a "pain syndrome." According to Chinese medicine, "pain syndrome" can be ascribed to either the pain of impassability or the vacuity heart pain of lusterlessness. Pivot Meridian Tuina therapy is a fundamental component of external treatment methods in traditional Chinese medicine. This therapy involves the gentle stimulation of specific acupoints on the patient's body. to address the underlying causes of pain, particularly focusing on alleviating both the pain of impassability and the vacuity heart pain of lusterlessness to achieve effective relief. In the

Huang Di Nei Jing, human body meridians are categorized into three groups: "open," "close," and "pivot." Among these, the open and close meridians are further associated with the concept of a "door." In this analogy, the Shujing represents the door shaft. It is widely acknowledged that the functionality of a door largely depends on its ability to open and close smoothly. Moreover, the concept of Shujing encompasses four specific meridians: the heart meridian of hand-shaoyin, the kidney meridian of foot-shaoyin, the triple energizer meridian of hand-shaoyang, and the gallbladder meridian of foot-shaoyang [14]. The treatment principle, based on Shujing theory, centers on regulating the body's overall qi flow. This approach entails selecting acupoints primarily based on the four mentioned meridians and utilizing the Five Shu points, Eight Confluence points, and other specific acupoints. These specific points facilitate the connection between internal organs, pivot the body's qi, and regulate yin and yang. As a part of the Shujing system, the gallbladder meridian of foot-shaoyang traverses the body's side, passing through numerous muscles and bones. The optimal functionality of muscles and bones relies on the harmonization of various bodily functions, especially the synchronization of qi and blood. Meridians act as conduits for the flow of qi and blood. Simultaneously, the acupoints along the Shujing are crucial in regulating pivotal points overseeing the overall circulation of qi and blood in the body. Specifically, these acupoints effectively alleviate discomfort associated with muscular rheumatism by addressing imbalances in the qi and blood within the gallbladder meridian. Therefore, the primary meridian targeted for intervention in cases of NPP is the gallbladder meridian of foot-shaoyang.

We employed interventions at the Huantiao, Yanglingquan, and Xuanzhong points along the gallbladder meridian of the foot-shaoyang. The Huantiao point, located at the intersection of the foot-shaoyang meridian, is renowned for its ability to soothe sinews, promote vascular circulation, alleviate wind-related discomfort, alleviate pain, and enhance the well-being of the waist and knees. Huang Huazhi *et al.* [15] employed massage and kneading at the Huantiao (GB30) point to realign nerve fibers in rats with the CCI model. This intervention notably increased PWT, PWL, and SFI, leading to analgesic effects and improved gait in the rats. The Yanglingquan point serves as the converging point for the gallbladder meridian of foot-shaoyang, the lower confluent acupoint of the gallbladder, and the influential point of tendons among the eight confluent points. Here, the qi and blood of the gallbladder meridian of foot-shaoyang gather and circulate. Lv Taotao *et al.* [16] improved fine motor skills in rats with peripheral nerve injuries by stimulating points such as Yanglingquan (GB34) through massage. Therefore, massaging the Yanglingquan point can enhance local blood circulation and aid in the breakdown and dilution of inflammatory mediators, effectively alleviating local pain symptoms. The Xuanzhong point serves as the foot-sanyang of the great network and is a convergence point for the body's marrow qi among the eight confluent points of marrow convergence. Chen Yuzhou *et al.* [17] discovered that electroacupuncture at the Xuanzhong point (GB39) improves the inflammatory response, reduces serum MMP-3 (matrix metalloproteinase-3) and MMP-9 levels in rats with adjuvant arthritis, and relieves pain.

5.2 Relationship Between NPP and OTUB1, DEPTOR, and mTORC1 Signaling Pathways

NPP, a prevalent chronic pain condition, typically arises from disorders, injuries, or abnormalities within the somatosensory nervous system [18]. Both central and peripheral injuries can induce NPP. However, some NPP cases with clear causes lack well-targeted treatments. Therefore, a broad classification of NPP into central and peripheral categories serves as an initial framework for understanding and addressing these complexities [19]. Recent advancements have significantly improved our understanding of the mechanisms underlying NPP. These developments have revealed that immune cell microglia become activated following peripheral and central nerve injuries. The immunomodulators released by activated microglia contribute to NPP maintenance. Furthermore, macrophages migrate to the affected nerves, producing pro-inflammatory cytokines [20], which also play an essential role in NPP generation. Studies have demonstrated a high correlation between NPP, neuroinflammation, and the immune system [21]. Moreover, the mTORC1 signaling pathway culminates in autophagy.

Autophagy, a cellular process in eukaryotes, entails the recycling and degradation of cellular components and exhibits remarkable conservation across species. Autophagy is of various types, including microautophagy, macroautophagy, and chaperone-mediated autophagy (CMA). The macroautophagy process is primarily mediated and regulated by proteins en-

coded by autophagy-related genes, which are categorized into four subgroups, including the ULK complex [20]. The ULK complex is regulated by mTORC1, which dictates its phosphorylation status. This regulation hinges on the binding and dissociation of mTORC1 from the ULK complex, consequently triggering macroautophagy in a dephosphorylated state [22]. Additionally, autophagy may be involved in NPP generation. Therefore, most studies have focused on the interplay between NPP and macroautophagy. Both macroautophagy and CMA are crucial in central nervous system injury lesions. These mechanisms exhibit a mutually reinforcing relationship, as they can compensate for reduced fluxes in one another by amplifying their respective processes [23]. Additionally, as a form of selective autophagy, CMA guides specific protein complexes to lysosomes [24]. Once these complexes reach the lysosomes, the chaperone-substrate protein conjugate binds to lysosome-associated membrane proteins, ultimately culminating in substrate protein degradation [25]. CMA and macroautophagy differ notably in cargo selection and delivery. CMA precisely targets substrate proteins featuring a pentapeptide motif for degradation, confining its degradative activity to proteins possessing this specific motif [26]. The study of the microautophagy mechanism faces limitations due to inadequate tools. Microautophagy involves the direct phagocytosis of cytoplasm through the invagination of the lysosomal membrane [27]. This process results in the formation of vesicles through internalization, followed by their degradation within the organelle's lumen [28]. A significant portion of the microautophagy process is regulated by ATG（Anti-Thymocyte Globulin） proteins. These proteins are generally categorized into two groups based on their role in microautophagy: the core group, which plays a role in advancing autophagosome formation, and the adaptor machinery, which governs the timing and location of autophagosome formation [27]. Autophagy in the mTORC1 signaling pathway can regulate the production of inflammatory factors, such as IL-1β. Furthermore, IL-1β is detected in the autophagosome lumen and intermembrane spaces, suggesting that its secretion and degradation may be autophagy-dependent. Moreover, increased autophagic flux notably promotes IL-1β production, necessitating caspase-1 activation and inflammasome formation. Furthermore, autophagy facilitates IL-1β release *via* the non-traditional AIM2 (absent in melanoma 2) inflammasome [29]. The preceding step in the mTORC1 signaling pathway involves the formation of the ULK1 protein complex.

In the mTORC1 pathway, the ULK1 protein complex comprises the ULK1 protein kinase, the autophagy-related protein ATG13, and the FIP200-interacting protein. ULK1 functions as a serine/threonine protein kinase, and there exist five homologs of ULK1: ULK1, ULK2, ULK3, ULK4, and STK36 (serine/threonine kinase 36). However, only ULK1 and ULK2 are implicated in autophagy regulation. Moreover, ULK1 and ULK2 share approximately 52% protein sequence identity and approximately 78% similarity within their kinase domains. Both proteins act on the same core components to regulate autophagy. Recent research has revealed that ATG13 and its heterodimer partner ATG101 facilitate the interaction between ULK1 and FIP200. Furthermore, ATG13 augments the interaction between ULK1 and FIP200 [30-32]. Moreover, FIP200 is a protein composed of 1,594 residues and comprises a dimeric N-terminal scaffolding structural domain, an IDR (intrinsically disordered region), a coiled-coil region, and a C-terminal claw structural domain. The C-shaped N-terminal structural domain dimer of the FIP200 scaffold assembles the ULK1 complex. ATG13 forms a HORMA (Named after Hop1p, Rev7p, and MAD2) dimer crucial for interacting with phosphatidylinositol-3-kinase (PI3K), which is essential for the function and assembly of the ULK1 complex [33]. Furthermore, both FIP200 and ATG13 enhance ULK1 kinase activity individually, but both are indispensable. Additionally, FIP200 serves as a scaffold protein for ULK1 and ATG13, playing key roles in their phosphorylation and stability. Additionally, both FIP200 and ATG13 are subject to upstream signaling by mTORC1, regulating autophagy through phosphorylation [34]. However, it is essential to note that ATG13 specifically belongs to the autophagy-related protein family.

Over 40 autophagy-related proteins have been identified and extensively studied in yeast, with over 20 of them being crucial in the autophagy process. These proteins are primarily categorized into six core functional groups. Most of these proteins have homologs in mammals [35]. In both plants and animals, the core ATG proteins can be categorized into four major complexes: the ATG1/ATG13 protein kinase complex, the ATG9/2/18 transmembrane complex, the PI3K complex, and the ATG5/ATG12 and ATG8-phosphatidylethanolamine coupling systems. The ATG1/ATG13 protein kinase complex is closely associated with the mTORC1 pathway. During the initial phase of autophagy, it initiates the phagocytosis of component groups based on the cell's nutrient requirements. Inacti-

vation of the TOR kinase results in ATG13 dephosphorylation, enabling its normal function. This dephosphorylation enhances ULK1 complex stability in the mTORC1 signaling pathway, subsequently facilitating downstream autophagic processes [36]. Various ATG proteins bind to and localize at the autophagy precursor structure, referred to as the pre-autophagosomal structure (PAS), a crucial component of autophagy. This docking structure serves as the initiation point for autophagy. FIP200, acting as a scaffold, plays a pivotal role in connecting ATG proteins to the PAS site, thereby facilitating their assembly and function in autophagy [37].

The interaction between mTORC1 and ATG13 plays a central role in regulating autophagy. In yeast, ATG13 functions as a direct substrate of mTORC1, which comprises the catalytic subunit of mammalian target of rapamycin (mTOR). As a sensor for cellular nutrient levels, both internally and externally, mTOR modulates various cellular processes, including cell growth and metabolism, to enhance cell survival in challenging conditions. Autophagy is one of the mechanisms through which TOR regulates these processes [38,39]. In a nutrient-rich environment, mTORC1 phosphorylates the Ser757 site of the ULK complex, leading to ULK1 phosphorylation. Simultaneously, mTORC1 also phosphorylates ATG13, a constituent of the ULK13 complex, at the Ser258 site. These actions collectively inhibit autophagy. However, when starvation is sensed by mTOR, mTORC1 becomes inactive. This inactivation allows for ULK1 activation through AMPK (AMP-activated protein kinase) dependent phosphorylation, thus triggering autophagy induction. The significance of mTORC1 in initiating autophagy is underscored by its regulation of the ULK1 complex [40]. Furthermore, within mTORC1, the mTOR-interacting protein DEPTOR contains DEP (Dishevelled, Egl-10, Pleckstrin) structural domains. As a part of the mTORC1 complex, DEPTOR naturally suppresses mTORC1, negatively influencing autophagy fluxes by downregulating the complex's activity [41].

Deptor (a monomeric protein, 46 kDa molecular weight) is encoded by the *DEPTOR* gene located on chromosome eight within the 8q24 region of the genome. Structurally, DEPTOR is characterized by three distinct and highly conserved domains: the DEP structural domain, composed of two N-terminal regions in tandem (residues 36–119 and 145–219), and the PDZ (Postsynaptic density 95, Discs large, Zonula occludens-1) structural domain, consisting of 78 amino acids (residues 330-407), located in the C-terminal region. Additionally, there is an approximately 100-residue unstructured junction (residues 228–323). DEPTOR is exclusively found in higher eukaryotes with a spine, while proteins containing the DEP structure exhibit significant structural and sequence similarity [42-44]. Functionally, DEPTOR serves as an endogenous negative regulator of mTORC1. However, its interaction with the mTOR differs from that of a distinct DEP structural domain. The unstructured junction of DEPTOR, also known as the long-chain subunit, interacts with mTOR FRB (FK-BP12-rapamycinbinding) domain, while the PDZ structural domains interact with the mTOR FAT (FAT-rapamycinbinding) domain. These interactions collectively inhibit mTORC1. However, even at the highest DEPTOR concentration, the mTORC1 complex retains about half of its kinase activity [45]. Additionally, DEPTOR, the sole protein modulator of the mTOR complex, has received limited research attention regarding its mechanism of molecular action. Nevertheless, studies have unveiled the presence of a phosphorylation motif within the junction connecting the DEP structural domain to the PDZ structural domain. This motif undergoes phosphorylation by mTOR, resulting in an additional phosphorylation event that activates the SCF (Skp1-cullin1-F-box-βTrCP) complex, an E3 ligase of the anaphase type, initiating polyubiquitination and subsequent degradation of DEPTOR. Moreover, this process can be counteracted by OTUB1, a protein containing the OUT (ovarian tumour) structural domain, which deubiquitinates DEPTOR, thus reversing its degradation [46,47].

Epigenetics is the field of study concerned with how various factors, especially environmental influences, can activate specific genes without altering the underlying DNA sequence, leading to changes in their expression and functional levels. Epigenetic modifications encompass chemical alterations involving DNA, RNA, and proteins. Among these modifications, the UB signaling system represents a specific type of chemical protein modification. UB consists of a class of highly conserved small molecular-weight proteins with an approximate molecular weight of 8.5 kDa. These proteins are ubiquitously present in all eukaryotic organisms [48]. Ubiquitination is a process in which UB (a 76-amino acid protein) is covalently attached to a protein substrate [49]. This attachment occurs through the covalent bonding of UB to a specific amino acid, typically lysine, on the target protein. The process involves consecutive actions performed by the UB-activating en-

zyme (E1), the UB-conjugating enzyme (E2), and the UB ligase (E3) [48,50-51]. Initially, UB attaches to E1 in an ATP-dependent manner, becomes activated, and is subsequently transferred to E2. Then, E2 also binds to UB and facilitates its transfer to E3. Finally, an isopeptide bond forms between the ε-amino group on the lysine residue of the target protein and the C-terminal Gly carboxylate group of UB. E3 plays a pivotal role in catalyzing this specific bonding between UB and the target protein, thereby facilitating the formation of an isopeptide bond [52,53]. UB frequently attaches to proteins with various lengths, diverse binding sites, and different structural arrangements. This diversity significantly contributes to the spectrum of posttranslational modifications (PTMs) in proteins, resulting in alterations in their crucial properties. These modifications impact their activity, cellular localization, interactions with other proteins, and, notably, their stability or half-life within the cell [49,54,55]. The UB signaling system has been extensively investigated and is recognized as a crucial mechanism for regulating numerous fundamental cellular processes. These biological processes encompass signal transduction, transcriptional regulation, protein degradation, epigenetic modifications, and intracellular localization [56]. Several studies have demonstrated the association of UB signaling with NPP development [57-59] and revealed that the UB system is a major determinant of pain responses in inflammatory pain and NP models.

Ubiquitination, a crucial PTM, plays a multifaceted role in regulating various cellular autophagy phases. Ubiquitination modifications participate in fundamental autophagic processes, including autophagosome membrane formation, amplification, maturation, and termination [60,61]. Additionally, ubiquitination modifications are integral to selective autophagy [62,63], wherein specific substrates, such as protein aggregates or damaged organelles, are recognized for lysosomal degradation through ubiquitination markers. These markers enable precise targeting of these substrates for autophagic degradation. The UB signaling system comprises ubiquitination and deubiquitination processes in a delicate equilibrium. Any imbalance within this system can disrupt target proteins, impacting their functionality and stability. In the maintenance of UB signaling system equilibrium, deubiquitinating enzymes (DUBs) play a crucial role. These enzymes, acting as specific proteases, hydrolyze UB linkages, countering UB signaling. Furthermore, they are pivotal for recycling and generating free UB within the cellular environment. This enables various ubiquitinases to attract target proteins towards them for degradation or signaling [64]. Moreover, DUBs regulate the entire autophagic process, encompassing both its initiation and the ultimate degradation of substrates. This is accomplished through targeting the ubiquitinated autophagy regulatory components [65,66].

OTUB1 is a fundamental component within the OTU deubiquitination superfamily, exerting its influence on both the NF-κB (Nuclear factor kB) and TGF-β (Transforming growth factor-β) signaling pathways [67]. Moreover, OTUB1 exhibits expression in various human tissues, predominantly in peripheral blood mononuclear cells, lymph nodes, spleen, and tonsils. Functionally, OTUB1 regulates immune responses, estrogen signaling, DNA damage response, and pathogen biology [68]. OTUB1 prefers binding with UB-carrying E2 enzymes, overlapping a binding surface with E3 enzymes. Consequently, this interaction between OTUB1 and E2 enzymes might contribute to the attenuation of E2-E3 binding [69,70]. In most cases, OTUB1 operates independently of its DUB activity. Include the regulation of DNA damage-induced chromatin ubiquitination [71], T-cell dysfunction [68], and SMAD2/3 signaling" for improved clarity modulation [67], suggesting that DUBs achieve deubiquitination by inhibiting UB-conjugating enzymes (E2). OTUB1 is expressed in most tissues, indicating it may undertake diverse cellular functions. Studies have revealed that OTUB1 can impede the ubiquitination modification of DEPTOR. Notably, its deubiquitination function does not rely on its deubiquitinating activity but instead operates through a non-classical pathway. Specifically, the presence of aspartic acid at position 88 in OTUB1 facilitates its binding to E2, effectively inhibiting its function. This interaction disrupts the formation of ubiquitination chains, consequently impeding the ubiquitination modification of substrate proteins [72]. This study revealed that OTUB1 inhibits mTORC1 activity by acting through DEPTOR, thereby impacting cellular autophagy.

5.3 Analysis of Experimental Results

5.3.1 Analysis of Behavioral Results

On the first postoperative day, the PWMT and PWTL in all groups exhibited lower values compared to the blank control group, indicating the successful implementation of the SNL modeling. By the third postoperative day, PWMT and PWTL

in the model, Pivot Meridian Tuina, sham massage, and NC groups had markedly decreased compared to the sham operation group. This observation suggests that the skin and muscle, being peripheral somatic tissues, can facilitate the transmission of nociceptive information to the superficial dorsal horn of the spinal cord through myelin-sheathed A-fibers and unmyelinated C-fibers. However, this transmission is not as pronounced as the pain induced in the SNL model. Moreover, compared to the model group, both the OTUB1 overexpression and the Pivot Meridian Tuina groups exhibited increased PWMT and PWTL values. Specifically, the OTUB1 overexpression group demonstrated a notable increase in PWMT, while the Pivot Meridian Tuina group exhibited a considerable elevation in PWTL. These findings indicate that the OTUB1 overexpression virus and the Pivot Meridian Tuina interventions exerted their effects. The therapeutic effects of Pivot Meridian Tuina appear to be initiated by restoring PWTL in SNL rats. Conversely, the therapeutic effect of the OTUB1 overexpression virus commences with the restoration of the PWMT in SNL rats. On the 14th postoperative day, both the PWMT and PWTL were increased in the Pivot Meridian Tuina and the OTUB1 overexpression groups compared to the model, sham massage, and NC groups. This indicates a significant improvement in the behavioral performance of SNL rats due to the notable impacts of Pivot Meridian Tuina and OTUB1 overexpression viruses. Relative to that in the model group, PWTL in the sham massage group was markedly elevated, while PWMT exhibited only a marginal increase. This suggests that the sham massage, essentially consisting of gentle stroking, might act as a placebo. This action potentially prevented the rats from becoming agitated and contributed to calming their disposition, thereby providing a minor degree of pain relief.

5.3.2 Analysis of Laboratory Results

5.3.2.1 Analysis of Western Blot Results

Relative to the blank control group, the model group exhibited decreased OTUB1 and DEPTOR expression, along with a notable elevation in mTORC1 expression. Following a 14-day Pivot Meridian Tuina intervention, OTUB1 and DEPTOR expression increased, while mTORC1 expression decreased. Compared to that in the NC group, OTUB1 and DEPTOR expression in the OTUB1 overexpression group were elevated. Moreover, mTORC1 expression was decreased in the OTUB1 overexpression group, suggesting that the OTUB1 overexpression group exhibited a similar response to the Pivot Meridian Tuina intervention. Compared to that in the model and sham massage groups, OTUB1 and DEPTOR expression were variably elevated, and mTORC1 expression was reduced, albeit with less pronounced fluctuations compared to the Pivot Meridian Tuina group. This underscores that sham massage, acting as a placebo, also had some influence on OTUB1, DEPTOR, and mTORC1 expression. However, the impact was not as significant as observed in the Pivot Meridian Tuina group. As the ubiquitination status of DEPTOR is dynamic, western blot detection revealed only slight differences in DEPTOR expression between the groups. However, these differences were not statistically significant (P>0.05). Consequently, further investigation was conducted to explore the ubiquitination status of DEPTOR.

5.3.2.2 Analysis of CO-IP Results

A. Results of the Deptor Ubiquitination Status Detection

Relative to that in the blank control group, UB binding in the model group decreased, indicating that the SNL model elevates DEPTOR levels in a deubiquitinated state. After a 14--day Pivot Meridian Tuina intervention, UB binding notably increased in the Pivot Meridian Tuina group, indicating an increased presence of DEPTOR in a deubiquitinated state in this group. Compared to that in the NC group, UB binding in the OTUB1 overexpression group was markedly increased, suggesting an elevated level of DEPTOR in a deubiquitinated state in this group. Therefore, the pattern observed in the Pivot Meridian Tuina group aligns with that of the OTUB1 overexpression group. Additionally, compared to the model group, the sham massage group exhibited a certain degree of increase in UB binding, signifying that the sham massage intervention influenced the deubiquitinated state of DEPTOR to some extent.

B. Results of the Ulk1 Complex Protein Expression Assessment

Compared to those in the blank control group, ULK1 and FIP200 levels in the model group exhibited a moderate decrease, though not significantly pronounced. This suggests that SNL exerts a limited influence on ULK1 and FIP200 lev-

els. Relative to those in the model group, ULK1 and FIP200 levels in the Pivot Meridian Tuina group were markedly elevated, indicating that Pivot Meridian Tuina induces ULK1 and FIP200 protein expression. Similarly, in the sham massage group, ULK1 and FIP200 levels exhibited varying degrees of increase compared to those in the model group. However, the expression of these proteins was not as pronounced as in the Pivot Meridian Tuina group. Therefore, notably, the calming effect of sham massage had a limited impact on ULK1 and FIP200 proteins. Relative to those in the NC group, ULK1 and FIP200 proteins in the OTUB1 overexpression group were markedly elevated. Consequently, the protein expression patterns in the Pivot Meridian Tuina group align with those in the OTUB1 overexpression group.

5.3.2.3 Analysis of ELISA Results

Serum IL-1β levels in all groups were higher compared to the blank control group, suggesting an upregulation in the expression of inflammatory factors following nerve, muscle, and skin injuries in the rats. Compared to those in the model group, serum IL-1β levels were significantly decreased in the Pivot Meridian Tuina group, indicating the therapeutic potential of Pivot Meridian Tuina in reducing the release of inflammatory factors. The sham massage group exhibited a decrease in serum IL-1β levels relative to the model group, implying that gentle caressing, functioning as a placebo, could also alleviate the release of inflammatory factors to some extent. However, when comparing the efficacy of the sham massage and Pivot Meridian Tuina groups in suppressing the release of inflammatory factors, the sham massage group demonstrated a notably reduced ability compared to the Pivot Meridian Tuina group. The OTUB1 overexpression group exhibited notably reduced levels of serum IL-1β compared to the NC group, aligning with the observations in the Pivot Meridian Tuina group.

6. Conclusion

Our findings demonstrate that (A) the SNL model considerably lowers both PWMT and PWTL. Moreover, Pivot Meridian Tuina mitigates these indicators in SNL model rats, effectively improving spontaneous pain and thermal hyperalgesia induced by nerve injury in rats. Additionally, it ameliorates nerve injury to varying degrees, providing relief from NPP-associated pain. (B) Pivot Meridian Tuina influences the deubiquitinating enzyme OTUB1 in spinal cord tissues, leading to alterations in the ubiquitination of DEPTOR, consequently regulating the downstream autophagy pathway. Consequently, these regulatory mechanisms contribute to the observed therapeutic effects in terms of inflammation inhibition and analgesia induction in NPP rats.

7. Shortcomings and Prospects

The intervention strength applied to the rats in this study was set at 4 N, a determination made solely through pre-training, which may have introduced potential errors in assessment. Additionally, we did not explore the impact of varying strengths on the pain threshold of the rats, indicating a limitation in its scope. To address this limitation, our team plans to acquire an instrument for visualizing these strengths in the future. This instrument will facilitate a comprehensive investigation into the impact of various manipulation strengths, including light, medium, and heavy forces, on rats experiencing pain.

We assessed ULK1 complex levels through co-IP, using ATG13 as the sole precipitating protein to quantify ULK1 and FIP200 protein levels. However, no reciprocal validation was performed for this complex. To enhance the comprehensiveness of our investigation, we propose conducting co-IP with FIP200 as the precipitating protein. This approach will facilitate the evaluation of ULK1 and ATG13 protein content, thus enabling the reverse validation necessary to identify the core protein within the complex.

Funding

This work was supported by the Guangxi University of Chinese Medicine 2022 Postgraduate Research Innovation Project (YCSW2022339), the Guangxi Natural Science Foundation (2023GXNSFAA026100), and the National Natural Science Foundation of China (82074574).

Author Contributions

Tianyi Wang was responsible for the design of the study protocol and animal modeling. Siqi Wu and Wang Yang organized the data and analyzed the experimental results. Yingye Liang ensured quality control and proofread the article. Hongliang Tang conceptualized the research, assumed overall

responsibility for the article, and provided supervision and management.

Conflict of Interest

Each author certifies that he or she, or a member of his or her immediate family, has no commercial association (i.e., consultancies, stock ownership, equity interest, patent/licensing arrangements, etc.) that might pose a conflict of interest in connection with the submitted manuscript.

References

1. Kankowski S, Grothe C, Haastert-Talini K (2021) Neuropathic pain: spotlighting anatomy, experimental models, mechanisms, and therapeutic aspects. Eur J Neurosci, 54: 4475-96.

2. Yang SB, Hu L, Chi XH, Zhang ZF (2021) Effect of Blood Nerve Barrier and Claudin-1 on Chronic Neuropathic Pain in Rats. [in Chinese] Neural Injury and Functional Reconstruction, 16: 67-70.

3. Du T, Yuan W, Cao B, et al. (2021) Chronic neuropathic pain. [in Chinese] Chinese Journal of Pain Medicine, 27: 481-5.

4. Corli O, Roberto A, Corsi N, Galli F, Pizzuto M (2019) Opioid switching and variability in response in pain cancer patients. Support. Care Cancer, 27: 2321-7.

5. Shaheen A, Alam SM, Azam F, et al. (2022) Lack of impact of OCTN1 gene polymorphisms on clinical outcomes of gabapentinoids in Pakistani patients with neuropathic pain. PLoS One, 17: e0266559.

6. Theken KN (2018) Variability in analgesic response to non-steroidal anti-inflammatory drugs. Prostaglandins Other Lipid Mediat, 139: 63-70.

7. Wang X, Liang Y, Lu D, et al. (2022) The effects of pivot meridian massage on the expression of VGLUT2 and inflammatory factors in chronic pain model. [in Chinese] Journal of Guangxi University of Chinese Medicine, 25:39-44.

8. Fu W, Tang H, Liang Y, et al. (2022) Effect of Shujing Tuina on Activation of NLRP3 Inflammation in Rats with Neuropathic Pain and Its Analgesic Mechanism. [in Chinese] Liaoning Journal of Traditional Chinese Medicine,49: 187-91.

9. Xing X, Xu F, Wang Y, Liu H (2023) Role of the OTUB1/IRF7/NOX4 axis in oxidative stress injury and inflammatory responses in mice with Parkinson's disease. Psychogeriatrics, 23: 32-44.

10. Wang Q, Lin J, Yang P, et al. (2020) Effect of Massage on the TLR4 Signalling Pathway in Rats with Neuropathic Pain. Pain Research & Management, 12: 1-6.

11. Xu C, Lin C (2019) Research progress of intrathecal tube operation in rats. [in Chinese] Chinese Journal of Pain Medicine, 25: 811-6.

12. Chen X, Li Z, Zhang B, et al. (2019) Alleviation of Mechanical allodynia by 14,15-epoxyeicosatrienoic acid in a central poststroke pain model: possible role of allopregnanolone and delta-subunit-containing gamma-aminobutyric acid A receptors. J Pain, 20: 577-91.

13. Shi Y, Wu W (2016) Treatment of Neuropathic Pain Using Pulsed Radiof- requency: A Meta-analysis. Pain Physician, 19: 429-444.

14. Pang J (2010) Study on Theory and Application of Doctrine of Axis Meridians. [Ph.D. dissertation] Hubei University of Chinese Medicine, Hubei.

15. Huang HZ, Lyu LJ, Liu Z, et al. (2023) Intervention effect of Tuina pressing and kneading the Huantiao (GB30) acupoint on NF-κB p65 protein at spinal cord dorsal horn in sciatica rats. [in Chinese] Zhongguo Gu Shang, 36: 519-24.

16. Lv T, Mo Y, Yu T, et al. (2020) An Investigation into the Rehabilitative Mechanism of Tuina in the Treatment of Sciatic Nerve Injury. Evid Based Complement Alternat Med, 2020: 5859298.

17. Chen YZ, Su CG, Chen TL, Chen YF, Li LB, Zhu J (2019) Electroacupuncture at "Zusanli"(ST36) and "Xuanzhong"(GB39) improves inflammatory reactions and reduces levels of serum MMP-3 and MMP-9 in adjuvant arthritis rats, 44: 659-62.

18. Finnerup NB, Kuner R, Jensen TS (2021) Neuropathic Pain: From Mechanisms to Treatment. Physiological Reviews, 101: 259-301.

19. Liao MF, Lu KT, Hsu JL, Lee CH, Cheng MY et al. (2022) The Role of Autophagy and Apoptosis in Neuropathic Pain Formation. Int J Mol Sci, 23:2685.

20. Shrivastava M, Ye L (2022) A Review on Autophagy in Orofacial Neuropathic Pain. Cells, 11: 3842.

21. Li J, Tian M, Hua T, et al. (2021) Combination of autophagy and NFE2L2/NRF2 activation as a treatment approach for neuropathic pain. Autophagy, 17: 4062-2.

22. Cao W, Li J, Yang K, Cao D (2021) An overview of autophagy: Mechanism, regulation and research progress. Bull Cancer, 108: 304-22.

23. Liao MF, Lu KT, Hsu JL, Lee CH, Cheng MY et al. (2022) The Role of Autophagy and Apoptosis in Neuropathic Pain Formation. Int J Mol Sci, 23: 2685.

24. Dong S, Wang Q, Kao YR, et al. (2021) Chaperone-mediated autophagy sustains haematopoietic stem-cell function. Nature, 591: 117-23.

25. Bourdenx M, Martín-Segura A, Scrivo A, et al. (2021) Chaperone-mediated autophagy prevents collapse of the neuronal metastable proteome. Cell, 184: 2696-714.e25.

26. Qiao L, Ma J, Zhang Z, et al. (2021)Deficient Chaperone--Mediated Autophagy Promotes Inflammation and Atherosclerosis. Circ Res, 129: 1141-57.

27. Sakai Y, Oku M (2023) ATG and ESCRT control multiple modes of microautophagy. FEBS Lett Published online.

28. Krause GJ, Cuervo AM (2021) Assessment of mammalian endosomal microautophagy. Methods Cell Biol, 164: 167-85.

29. Ge Y, Huang M, Yao YM (2018) Autophagy and pro-inflammatory cytokines: Interactions and clinical implications. Cytokine & Growth Factor Reviews, 43: 38-46.

30. Wong PM, Puente C, Ganley IG, Jiang X (2013) The ULK1 complex: sensing nutrient signals for autophagy activation. Autophagy, 9: 124-37.

31. Lin MG, Hurley JH (2016) Structure and function of the ULK1 complex in autophagy. Curr Opin Cell Biol 2016;39:61-68.

32. Zachari M, Ganley IG (2017) The mammalian ULK1 complex and autophagy initiation. Essays Biochem, 61: 585-96.

33. Shi X, Chang C, Yokom AL, Jensen LE, Hurley JH (2020) The autophagy adaptor NDP52 and the FIP200 coiled-coil allosterically activate ULK1 complex membrane recruitment. Elif, 9: e59099.

34. Ganley IG, Lam du H, Wang J, Ding X, Chen S, Jiang X (2009) ULK1.ATG13.FIP200 complex mediates mTOR signaling and is essential for autophagy. J Biol Chem, 284: 12297-305.

35. Cai YY, Li L, Zhu XM, Lu JP, Liu XH et al. (2022) The crucial role of the regulatory mechanism of the Atg1/ULK1 complex in fungi. Front Microbiol, 13: 1019543.

36. Zhou Y, Manghwar H, Hu W, Liu F (2022) Degradation Mechanism of Autophagy-Related Proteins and Research Progress. Int J Mol Sci, 23: 7301.

37. Li X, He S, Ma B (2020) Autophagy and autophagy-related proteins in cancer. Mol Cancer, 19: 12.

38. Rabanal-Ruiz Y, Otten EG, Korolchuk VI (2017) mTORC1 as the main gateway to autophagy. Essays Biochem, 61: 565-84.

39. Noda T (2017) Regulation of Autophagy through TORC1 and mTORC1. Biomolecules, 7:52.

40. Han X, Goh KY, Lee WX, Choy SM, Tang HW (2022) The Importance of mTORC1-Autophagy Axis for Skeletal Muscle Diseases. Int J Mol Sci, 24: 297.

41. Morales-Martinez M, Lichtenstein A, Vega MI (2021) Function of Deptor and its roles in hematological malignancies. Aging (Albany NY), 13: 1528-64.

42. Catena V, Fanciulli M (2017) Deptor: not only a mTOR inhibitor. J Exp Clin Cancer Res, 36: 12.

43. Caron A, Briscoe DM, Richard D, Laplante M (2018) DEPTOR at the Nexus of Cancer, Metabolism, and Immunity. Physiol Rev, 98: 1765-803.

44. Perez-Tejeiro JM, Csukasi F (2021) DEPTOR in Skeletal Development and Diseases. Front Genet, 12: 667283.

45. Heimhalt M, Berndt A, Wagstaff J (2021) Bipartite binding and partial inhibition links DEPTOR and mTOR in a mutually antagonistic embrace. Elife, 10: e68799.

46. Wälchli M, Berneiser K, Mangia F (2021) Regulation of human mTOR complexes by DEPTOR. Elife, 10: e70871.

47. Thompson LL, Rutherford KA, Lepage CC, McManus KJ (2021) The SCF Complex Is Essential to Maintain Genome and Chromosome Stability. Int J Mol Sci, 22: 8544.

48. Husnjak K, Dikic I (2012) Ubiquitin-binding proteins: decoders of ubiquitin-mediated cellular functions. Annu Rev Biochem, 81: 291-322.

49. Hershko A, Ciechanover A (1998) The ubiquitin system. Annu Rev Biochem, 67: 425-79.

50. Lopez-Castejon G (2020) Control of the inflammasome by the ubiquitin system. FEBS J, 287: 11-26.

51. Akutsu M, Dikic I, Bremm A (2016) Ubiquitin chain diversity at a glance. J Cell Sci, 129: 875-80.

52. Klionsky DJ, Petroni G, Amaravadi RK, Baehrecke EH, Ballabio A, et al. (2021) Autophagy in major human diseases. EMBO J, 40: e108863.

53. Lamark T, Johansen T (2021) Mechanisms of selective autophagy. Annu Rev Cell Dev Biol, 37: 143-69.

54. Lacoursiere RE, Hadi D, Shaw GS (2022) Acetylation, Phosphorylation, Ubiquitination (Oh My!): Following Post--Translational Modifications on the Ubiquitin Road. Biomolecules, 12: 467.

55. Zheng N, Shabek N (2017) Ubiquitin Ligases: Structure, Function, and Regulation. Annu. Rev. Biochem, 86: 129-57.

56. Kowalski JR, Juo P (2012) The role of deubiquitinating enzymes in synaptic function and nervous system diseases. Neural Plasticity, 2012: 892749.

57. Li J, Tian M, Hua T, Wang H, Yang M, et al. (2021) Combination of autophagy and NFE2L2/NRF2 activation as a treatment approach for neuropathic pain. Autophagy, 17: 4062-82.

58. Sun L, Tong CK, Morgenstern TJ, Zhou H, Yang G, et al. (2022) Targeted ubiquitination of sensory neuron calcium channels reduces the development of neuropathic pain. Proc Natl Acad Sci USA, 119: e2118129119.

59. Cheng J, Deng Y, Zhou J (2021) Role of the Ubiquitin System in Chronic Pain. Front Mol Neurosci, 14: 674914.

60. Nakatogawa H, Ichimura Y, Ohsumi Y (2007) Atg8, a ubiquitin-like protein required for autophagosome formation, mediates membrane tethering and hemifusion. Cell, 130: 165-78.

61. Antonioli M, Di Rienzo M, Piacentini M, Fimia GM (2017) Emerging mechanisms in initiating and terminating autophagy. Trends Biochem Sci, 42: 28-41.

62. Khaminets A, Behl C, Dikic I (2016) Ubiquitin-dependent and independent signals in selective autophagy. Trends Cell Biol, 26: 6-16.

63. Rogov V, Dötsch V, Johansen T, Kirkin V (2014) Interactions between autophagy receptors and ubiquitin-like proteins form the molecular basis for selective autophagy. Mol. Cell, 53: 167-78.

64. Park CW, Ryu KY (2014) Cellular ubiquitin pool dynamics and homeostasis. BMB Rep, 47: 475-82.

65. Liang JX, Ning Z, Gao W (2014) Ubiquitin-specific protease 22-induced autophagy is correlated with poor prognosis of pancreatic cancer. Oncol Rep, 32: 2726-34.

66. Pukaß K, Richter-Landsberg C (2015) Inhibition of UCH-L1 in oligodendroglial cells results in microtubule stabilization and prevents α-synuclein aggregate formation by activating the autophagic pathway: Implications for multiple system atrophy. Front. Cell. Neurosci, 9: 163.

67. Herhaus L, Al-Salihi M, Macartney T, Weidlich S, Sapkota GP (2013) OTUB1 enhances TGFβ signalling by inhibiting the ubiquitylation and degradation of active SMAD2/3. Nat Commun, 4: 2519.

68. Soares L, Seroogy C, Skrenta H, Anandasabapathy N, Lovelace P, et al. (2004) Two isoforms of otubain 1 regulate T cell anergy via GRAIL. Nat Immunol, 5: 45-54.

69. Juang YC, Landry MC, Sanches M (2012) OTUB1 co-opts

Lys48-linked ubiquitin recognition to suppress E2 enzyme function. Mol Cell, 45: 384-97.

70. Wiener R, Zhang X, Wang T, Wolberger C (2012) The mechanism of OTUB1-mediated inhibition of ubiquitination. Nature, 483: 618-22.

71. Nakada S, Tai I, Panier S (2010) Non-canonical inhibition of DNA damage-dependent ubiquitination by OTUB1. Nature, 466: 941-6.

72. Zhao L, Wang X, Yu Y (2018) OTUB1 protein suppresses mTOR complex 1 (mTORC1) activity by deubiquitinating the mTORC1 inhibitor DEPTOR. J Biol Chem, 293: 4883-92.